Triangles on a triangular lattice: Insights into self-assembly in two dimensions driven by shape complementarity

S. S. Akimenko,* A. V. Myshlyavtsev, M. D. Myshlyavtseva, V. A. Gorbunov, S. O. Podgornyi, and O. S. Solovyeva
Department of Chemistry and Chemical Engineering, Omsk State Technical University, Mira Avenue 11, Omsk 644050, Russian Federation

(Received 28 September 2021; accepted 7 March 2022; published 4 April 2022)

A series of models for reversible filling of a triangular lattice with equilateral triangles has been developed and investigated. There are eight distinct models that vary in the set of prohibitions. In zeroth approximation, these models allow one to estimate the influence of the particles' shape and complementarity of their pair configurations on the self-assembly of dense monolayers formed by reversible filling. The most symmetrical models were found to be equivalent to hard-disk models on the hexagonal lattice. When any contact of hard triangles by vertices is prohibited, the dense monolayers are disordered, and their entropy tends to the constant. If only one pair configuration is prohibited, the close-packed layer appears through the continuous phase transition. In other cases, the weak first-order transition resulting in the self-assembly of close-packed layers is observed.

DOI: 10.1103/PhysRevE.105.044104

I. INTRODUCTION

Understanding the self-assembly of many particles leading to ordered structures of larger scale is the inevitable milestone in the technological development of our civilization. Firstly, it is potentially a highly effective way manufacture new materials. Secondly, it is a way to create entirely new functions and technological capabilities inspired by living organisms. The shape of the assembling objects (or interacting particles) is the most important factor in our understanding of the self-assembly. The shape significantly affects the geometry of close packing, directionality, and selectivity of interaction between particles [1–4], often regardless of scale. Any shape arises from breaking the spherical symmetry of an object and is usually determined by the geometry of its surface. Therefore, a shape is usually defined by a set of short-range repulsive interactions between atoms on the object surface. Driven by such interactions the particles form ordered structures which fill space in the most efficient way and correspond to the minimum of relevant free energy of the system. In the case of "hard" particles the type of close packing is dominated by entropic contributions [1,3,5–7]. For example, spherical particles usually self-organize into cubic or hexagonal close-packed structures, while cubic particles form the simple cubic lattice. Self-assembly of triangular particles is much more difficult [7–10].

Considering the self-assembly of molecules and nanoscale objects, we inevitably take into account many different types of interactions. Functionalized organic molecules [11–14] or colloid particles [2,4,15–17] forming complex ordered structures clearly illustrate the point. The functionalization gives rise to the directionality of the interactions. In this case, the interaction force depends on the relative positions and orientations of the particles and achieves a maximum when the particles are complementary. Thus, defective and/or functionalized objects having the same tangible shape can interact in completely different ways. The resulting supramolecular structures will differ. Selective functionalization of nanoparticle faces has been adopted to nanochemistry to control the resulting nanostructures [18]. On the other hand, the "perfection" of the species' shape and structure is a necessary condition for the most complex self-assembly systems, including living organisms [19].

The hard-core lattice gas model is very important for understanding the influence of nanoparticles' or molecules' shape on their self-assembly and critical behavior. A suitable choice of the lattice, size, and shape of the excluded volume allows one, at least in principle, to determine the structure of close packing for almost any particle shape and reveal various phases appearing as the density increases [5]. Since in the hard-core lattice systems there are only infinite (excluding) or zero (allowing) interactions, temperature plays no role. Therefore, the phase transitions occurring in such systems are always entropy driven. In this case, ordered close-packed structures have a higher entropy than disordered ones under given conditions [5].

Two-dimensional lattice models of packing the particles of many different shapes have been studied. Examples include disks [20–29], triangles [10,30,31], squares [32–40], dimers [36,41–43], rectangles [37,44–46] and rods [47–51], Y-shaped particles [52], and hexagons [53]. Among them only the hard hexagon model is exactly solvable. For hard-core lattice gases of arbitrary geometry and wide range of density the equations of state have been derived [34,54–57]. Recently, multiple phase transitions have been discovered in several hard-core models with both symmetric and asymmetric particles. This phase behavior is associated with the formation of columnar and hexatic phases [22,25,26,36,44,52].

In this paper, we consider the self-assembly of triangles on a triangular lattice. The self-assembly of triangular particles is a general problem occurring at different scopes. One of

*akimenkosergey@mail.ru

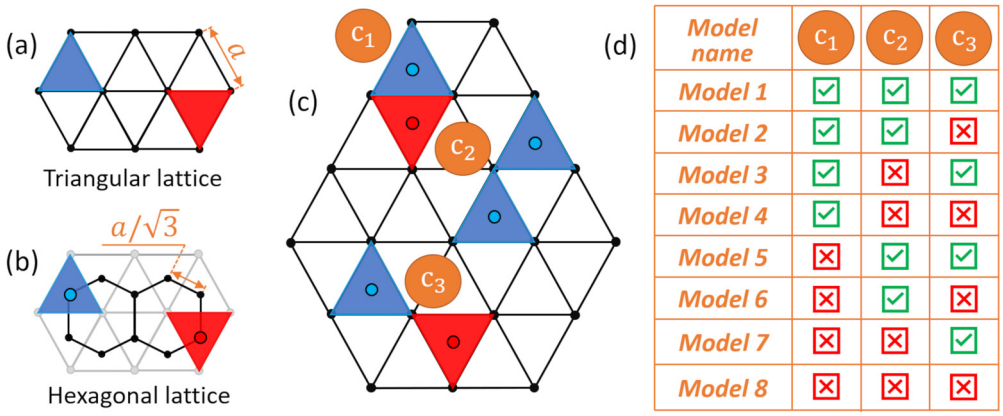

Model name	c_1	c_2	c_3
Model 1	☑	☑	☑
Model 2	☑	☑	☒
Model 3	☑	☒	☑
Model 4	☑	☒	☒
Model 5	☒	☑	☑
Model 6	☒	☑	☒
Model 7	☒	☒	☑
Model 8	☒	☒	☒

FIG. 1. The model visualization: (a) Possible orientations of triangles on a triangular lattice, (b) on a hexagonal lattice, (c) possible paired configurations, and (d) possible models.

the relevant examples is experimental and theoretical study of self-assembling adsorption monolayers of functional organic molecules having C_3 symmetry [11–14,58–67], which is important for development of organic electronics, sensors, and catalysis. Another well-known example is the self-assembly of colloidal crystals from nanoparticles of various shapes, including triangular [4,7,8,15,16,68]. In Sec. II we describe a series of lattice models for filling a triangular lattice with equilateral triangles. A difference between the models lies in the set of prohibited and allowed pair configurations. This is the simplest way to investigate the influence of the shape complementarity and functionalization of particles on the self-assembly of the close-packed layer. It can be considered as a zero approximation.

II. MODEL

The model describes reversible filling of a triangular lattice with equilateral triangles with side length equal to the lattice constant a. The vertices of the triangles are always located at the lattice sites. Therefore, the triangle can have two different orientations on the lattice [Fig. 1(a)]. Hereinafter the orientation of triangles is marked with color for clarity. Owing to the duality of triangular and hexagonal lattices, we can consider the centers of triangles being located at the sites of the hexagonal lattice [Fig. 1(b)] with a lattice constant equal to $a_h = a/\sqrt{3}$. Thus, for certain sets of prohibited and allowed pair configurations the model of triangles on the triangular lattice is assumed to be isomorphic to one of the hard-disk lattice gas models on the hexagonal lattice. Further, we will refer to this feature of the considered models and, if it is possible, compare the obtained results with the work [24].

In the described model the triangles can form three possible pair configurations on the triangular lattice: c_1, c_2, and c_3 [Fig. 1(c)]. Here, we will consider the model in terms of "prohibited" and "allowed" pair configurations and not account for any finite interaction. In a zeroth approximation, we study the influence of the particle shape complementarity on the self-assembly of dense monolayers formed by reversible filling. There are eight different special cases of the considered model depending on the combination of the prohibited and allowed pair configurations [Fig. 1(d)]. Further, we will refer to these cases as separate models. Each of them has real molecular [11,14,58,61] or nanoscale (colloidal) [4,7,15] prototypes differing in the particle shape or in the relevant functionalization or protection of the particle edges and vertices. The thermodynamic Hamiltonian of each model is written as the sum of occupied lattice sites multiplied by the chemical potential μ. For simplicity, we assume $\beta = (kT)^{-1} = 1$ in all calculations, where k is the Boltzmann constant and T is the absolute temperature. Below, we briefly describe the models.

Model 1. The model allows any contacts between the triangles excluding overlaps. This model is evidently isomorphic to the Langmuir model. In this regard, we will not study this model since it will not provide new results. The close-packed phase in this model has the maximum density due to the absence of any prohibited pair configurations. In this regard, we will use it as a density unit and, further, all the obtained densities will be normalized to this value.

Models 2–4. In these models, side-to-side pair configuration is allowed. The prohibitions on the contacts of triangles by the vertices vary from one model to another. There are no analogs of these models among the hard-disk models on the hexagonal lattice. Prohibiting one or two vertex-to-vertex pair configurations leads to a reduction of the model symmetry in comparison with model 1. Thus, the effect of shape complementarity of the particles is examined.

Model 5. Any contacts of the triangles by the vertices are allowed. In fact, there is a prohibition on nearest neighboring on the hexagonal lattice sites (1NN model). Therefore, this model is isomorphic to the hard-disk model on the hexagonal lattice. The model is known to possess one continuous phase transition belonging to the Ising universality class [24,27,69,70].

Model 6. In this instance the triangles having the same orientation can contact by vertices. Like models 2–4, it is not isomorphic to any hard-disk model on the hexagonal lattice. Therefore, it has not been studied previously.

Model 7. The triangles having opposite orientation are allowed to contact by vertices, but the side-to-side contact is prohibited. This model is isomorphic to the second nearest neighbor (2NN) model on the hexagonal lattice. In addition, this specific case of the general model can be interpreted as

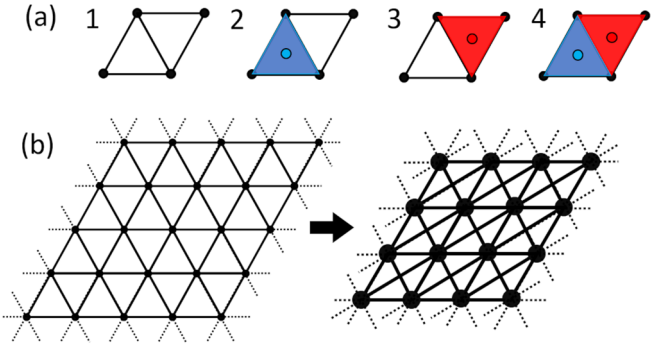

FIG. 2. Transformation of the lattice sites: (a) New states of the site, and (b) transformation of the lattice.

a model of Y-shaped molecules on the hexagonal lattice in which the weak first-order transition is observed [24].

Model 8. In this case of the general model, all contacts between the triangles are prohibited. That can be called "a hard triangles model on a triangular lattice." It is isomorphic to the third nearest neighbor (3NN) model on the hexagonal lattice. As is known, there is no phase transition in this model [24].

III. METHODS

The models were studied with the transfer matrix (TM), the tensor renormalization group (TRG), and the Monte Carlo (MC) methods. Such a set of methods allows one to minimize errors associated with the disadvantages of each methods used and to conduct a comprehensive study of the model. Calculations were carried out using SUSMOST 1.1 [71]. Below we briefly describe the details of each method.

Transfer-matrix method. The main idea of the method is to determine the partition function of a semi-infinite system ($M \times \infty$ sites) by calculating the largest eigenvalue of the transfer matrix describing the interactions between M sites. In addition, the eigenvectors of the transfer matrix allow one to estimate the probabilities of the corresponding configurations. It can be used to explore the structure of resulting phases. The main and well-known drawback of the TM method is the exponential growth of the computing time with increasing M. Thus, using the TM method it is possible to calculate thermodynamic characteristics of relatively small systems as well as assess the related size effects. A correct choice of M requires knowing in advance the structure of the phases which appear in the simulation at the considered conditions. The main advantage of the TM method is the ability to calculate any thermodynamic quantities (including entropy and heat capacity) with any desired accuracy for a semi-infinite system ($M \times \infty$). In this work, we used the mentioned features of the method to estimate the phase transitions.

To increase the limiting size of the studied system we have developed a less versatile code exploiting the system peculiarities. Let us briefly describe the main features of the TM algorithm used. Initially, the sites of the lattice are redefined in such a way that the new site is formed by joining two adjacent triangles on the original lattice [Fig. 2]. There are four different states of the new site: empty, the first triangle is filled, the second triangle is filled, and both triangles are filled.

Rings necessary for the implementation of the TM method are generated by sequentially adding sites of the new type. Accounting for numerous prohibitions on the nearest neighboring, this technique drastically reduces the number of preliminary computations by discarding the prohibited states at each step of the ring generation. Additional consideration of the translation invariance of the generated rings reduces the dimension of the resulting transfer matrix by about M times. Here M is the number of new sites in the ring. It allowed us to carry out the TM calculations at sufficiently large values of $M = 12-16$.

Tensor renormalization group. Designing the network was carried out as described in [23]. We performed the calculation according to the standard algorithm proposed by Levin and Nave [72]. A singular decomposition of the tensor T was further implemented, with only χ remaining of the largest singular values. In this way we had discarded configurations having the lowest probabilities. Next, the resulting tensors were contracted in the appropriate way. The resulting tensor T' described a system twice as large. The process was repeated until convergence on the partition function had been achieved. In fact, we had determined the partition function of the system. It can be further used to calculate any thermodynamic characteristics of the infinite system. The main problem of the TRG method lies in the difficulty of the error estimation. Therefore, the sufficient value χ is unknown in advance. In this work, the χ value was varied from 48 to 200. The maximum values of χ used in a particular calculation are indicated in all graphs. The difference in the partition function values obtained at various χ was used as the selection criterion as recently suggested in [23]. Thus, the TRG method had provided us the thermodynamic characteristics of the model guaranteed to be "clean" of the finite size effects. It was the main value of the TRG method in this study.

Monte Carlo method. The standard grand canonical Monte Carlo (GCMC) method as implemented in SUSMOST 1.1 was used for the simulations. To enhance the convergence to the equilibrium state we utilized the parallel tempering technique at $\beta = [0.83, 1, 1.25, 2.03, 3.32, 5]$. The elementary acts (adsorption, desorption, rotation, and diffusion) and temperature

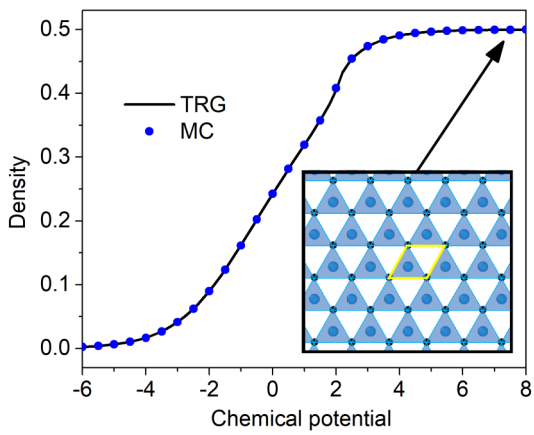

FIG. 3. Adsorption isotherm and lattice snapshot of model 5.

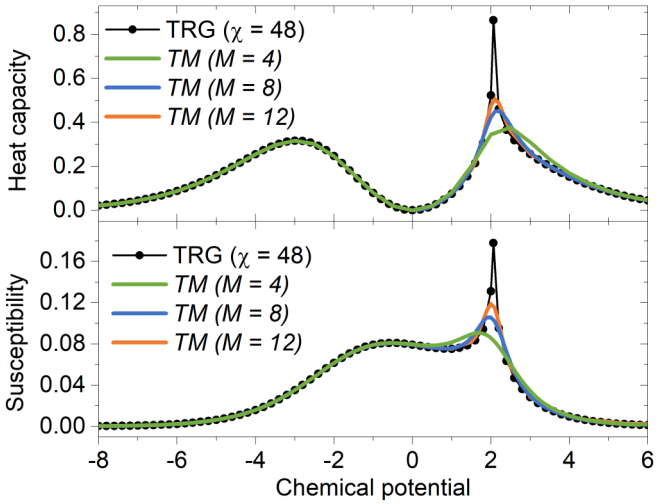

FIG. 4. Heat capacity and susceptibility of the layer vs chemical potential in model 5.

switching between the simulated systems were done according to the Metropolis algorithm. To equilibrate the system and calculate the average value of the density we performed 5.2×10^5 Monte Carlo steps. The size of the simulated system was $L = 60 \times 60$ in all cases. The GCMC method was mainly used for visual analysis of the layer structure and estimation of the layer density at key values of the chemical potential μ. Comparison of the layer densities obtained by the GCMC and TRG methods had allowed us to conclude whether the selected system size and the number of GCMC steps were sufficient or not.

IV. RESULTS AND DISCUSSION

The obtained results are discussed in two parts. In the first part, we consider the models that are isomorphic to hard-disk models on the hexagonal lattice: model 5 (1NN), model 7 (2NN), and model 8 (3NN). Those models were previously well studied [24], so we only compare the results and highlight previously unknown features. In the second part of the section, we consider the models having no consistent analogs on the hexagonal lattice. However, those models reveal the effect of particle shape anisotropy on the formation of dense monolayers from the lattice gas phase.

Model 5. As mentioned earlier, if we consider model 5 within the hexagonal lattice, then in fact we deal with the hard-disk model with the nearest neighbor exclusion. Figure 3 shows the layer density dependence on the chemical potential (hereinafter referred to as the "adsorption isotherm") and snapshots of the layer obtained by the GCMC method. In all cases, we preliminarily processed the images and show only a part of the lattice. The unit cell of the close-packed phase is marked in yellow.

In model 5, the close-packed phase consisting of identically oriented triangles is formed. A continuous phase transition belonging to the 2D Ising universality class is known to occur in this model. The approximate value of the critical chemical potential $\mu_c \approx 2.064$ [24] was also estimated in the previous studies. The dependences of the heat capacity C_V and density derivative on the chemical potential $\partial\theta/\partial\mu$ (or susceptibility) obtained by the TM and TRG methods are illustrated in Fig. 4. As one can see, an increase of the system size leads to convergence of the curves calculated by the TM and TRG methods.

Position of the heat capacity peak estimated by the TM method always lies to the right of the critical chemical potential μ_c, but the corresponding maximum of the susceptibility is always to the left. It allows one to find the boundary for the true value of the critical chemical potential. Using the scaling relation $\mu_M = \mu_c + a(M^{-2})$, where a is a constant, further improves the accuracy of such estimation. Thus, the TM method provides the following value of the critical chemical potential $\mu_c^{\mathrm{TM}} \approx 2.06 \pm 0.006$. It reproduces well the known result. The TRG method yields the value $\mu_c^{\mathrm{TRG}} \approx 2.06 \pm 0.005$.

Model 7. The model is equivalent to the hard-disk model on the hexagonal lattice with the first and second neighbor exclusion. Figure 5 shows the adsorption isotherm and layer images at full coverage of the lattice. The coexistence of two energetically equivalent phases is clearly observed in the close-packed layer. One of the phases exists as islands, while the elements of the other phase form the interface between those islands.

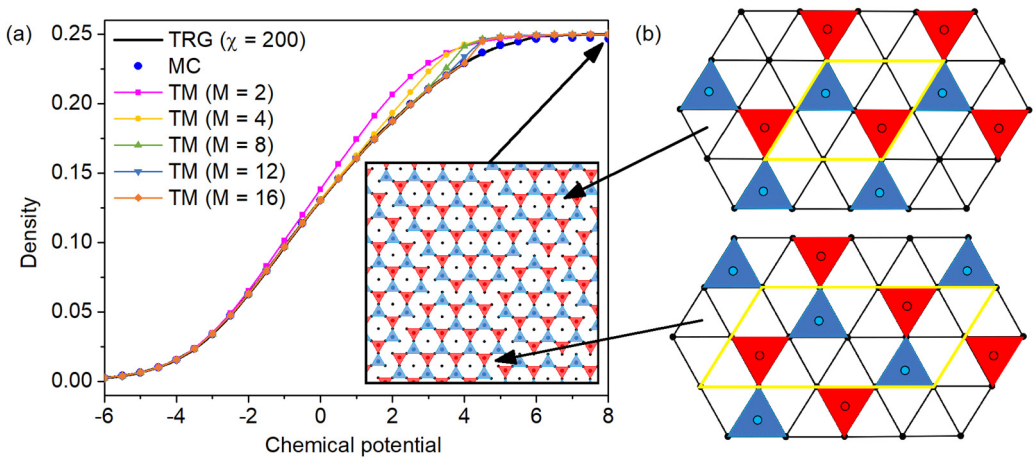

FIG. 5. (a) Adsorption isotherm and layer snapshot for model 7, and (b) structure of two energetically equivalent close-packed phases.

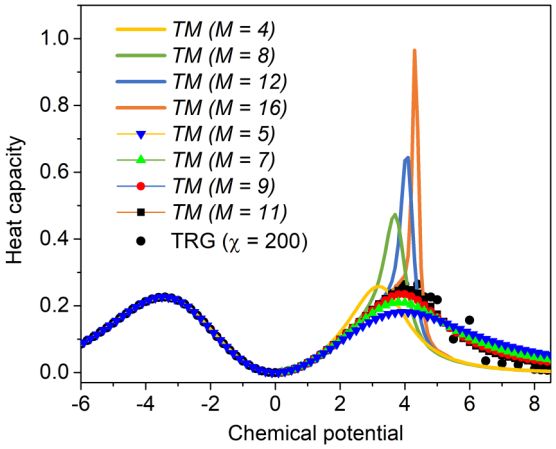

FIG. 6. Heat capacity vs chemical potential for model 7.

Recently, a weak first-order phase transition was revealed in this model [24]. Figure 6 illustrates the calculated dependence of the heat capacity on the chemical potential. Since the susceptibility curve behaves in a similar way, we do not demonstrate it here and further. Serious problems with accuracy of the TRG calculations are also seen in the figure. It can be associated with the degeneracy of the resulting dense structure. In the case of the infinite system, the peak should probably be observed in an infinitely small region of the chemical potential. This circumstance locks the determination of the critical value of the chemical potential for model 7 by the TRG method.

The data obtained with the TM method show sharp peaks at even values of M. Heights of the peaks noticeably grow, and the width decreases with increasing M. Such behavior is characteristic of a first-order phase transition. The heat capacity curves calculated at odd values of M differ from the even ones. Changes associated with increase of odd M are small, but the extremum gradually forms. The position and shape of the peak obtained at odd M approach the ones at even values of M. The described behavior results from the size of the unit cells of close-packed phases [Fig. 5(b)].

Since the position of the heat capacity peaks strongly depends on M, it hampers an accurate estimation of the critical chemical potential using the TM method. In this case, the shift of the peak position is determined not by a term proportional to M^{-d}, but by a term proportional to $M^{-(d-1)}$, where d is the space dimension [24]. The anomalous scaling dependence of the critical point position can be associated with the infinite degeneracy of the close-packed phase. This means that the entropy for a lattice of size $L \times L$ at $L \to \infty$ also tends to infinity according to a power law as L^{γ}, where $0 < \gamma \leqslant 2$. Direct TM calculation of the dimensionless entropy per one row at $\mu \to \infty$ results in the value $\ln 2/2$ and does not reveal any dependence on the TM ring size at $M \geqslant 4$. Thus, the exponent γ for model 7 is equal to 1 and the critical point position should be determined according to the anomalous scaling formulas.

We have approximated the critical value of the dimensionless chemical potential μ_c by $\mu_M = \mu_c + a(M^{-1}) + b(M^{-2})$, where a and b are constants. For $M = 8, 10, 12$ we have $\mu_c \approx 5.3$, which sufficiently differs from the value $\mu_c \approx 6.66$ obtained in [24]. For the next approximation at $M = 10, 12, 14$ we have found $\mu_c \approx 5.43$. The TM calculations at $M = 12, 14, 16$ have yielded $\mu_c \approx 5.65$. These results confirm the slow convergence with increasing M, which is characteristic of systems with infinite degeneracy of the ground state.

Model 8. Calculations carried out by all three methods unambiguously indicate the absence of phase transitions in this model. As seen on the snapshots collected in the GCMC simulation [Fig. 7(a)] there is no ordered structure of the layer. Instead, a mixture of differently oriented triangles is observed on the lattice. Figure 7 shows the adsorption isotherms, the heat capacity, and entropy dependences on the chemical potential.

The curves calculated with the TM method at $M \geqslant 8$ are practically independent of the M value, and a sharp peak is absent in all cases. This indicates the absence of phase transitions in this model. This behavior is known, but rather curious, since this model is equivalent to the 3NN model on the hexagonal lattice. It is known that for the kNN models on square and triangular lattices at any value of k, at least one

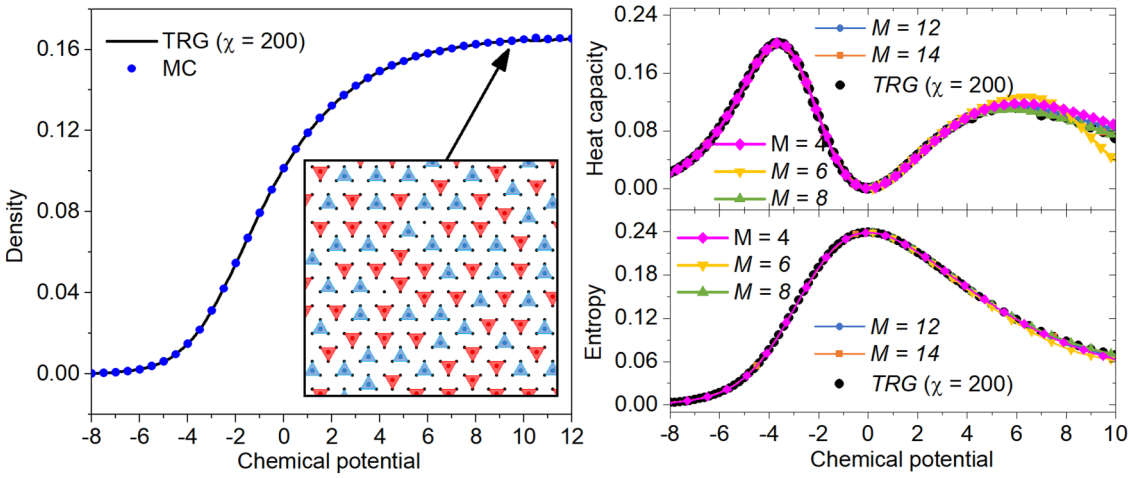

FIG. 7. Model 8: Adsorption isotherm, layer snapshot, and heat capacity and entropy vs chemical potential.

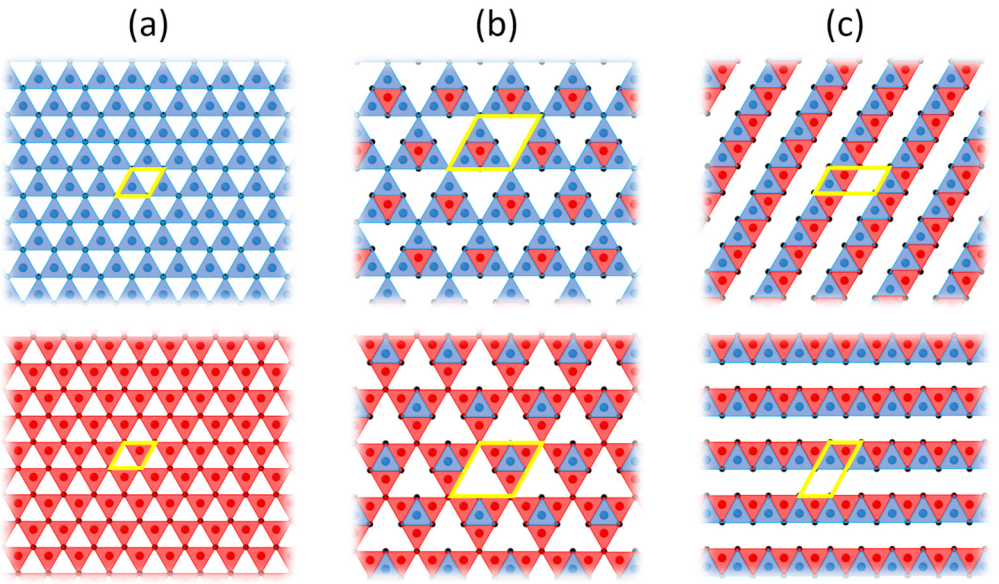

FIG. 8. Snapshots of close-packed phases appearing in model 2: (a) Triangle phase, (b) supratriangle phase, and (c) linear phase.

phase transition is always present, but the hexagonal lattice is different [24].

An interesting feature is the behavior of entropy per site at high density. It is equal to a nonzero value resulting from the disordered structure of the dense layer. For the same reason the TRG calculations at high density require a greater number of singular values. The entropy $S^{\mathrm{TRG}} = 0.045 \pm 0.001$ of the close-packed layer obtained with the TRG method is in good agreement with the limiting value $0.04-0.045$ of entropy calculated with the TM method.

Next, we consider the models that have no analogs among the models of hard disks on the hexagonal lattice and, therefore, have not been previously studied.

Model 2. We have found that this model is very similar to model 5, but not equivalent. It follows from the coincidence of the isotherms obtained with the TRG and GCMC methods, as well as the susceptibility, entropy, and heat capacity calculated with the TRG method. But the same accuracy of the TRG calculations for model 2 requires more singular values. The physical reason for this similarity is illustrated in the GCMC snapshots of close-packed structures observed in model 2 [Fig. 8].

The point is that one of the close-packed structures in model 2 coincides with the dense layer forming in model 5. Apparently, it is the reason for the similar behavior of the models. For deeper understanding of this phenomenon, we have compared the TM results obtained for both models at different values of M. Since the other characteristics behave in the same way, we demonstrate only the susceptibility curves [Fig. 9]. All the calculated thermodynamic characteristics of both models (isotherm, susceptibility, entropy, and heat capacity) are identical at the odd values of M. Such values of M force the appearance of the triangular phase consisting of identically oriented triangles. Other ordered structures are not formed in model 2 at odd M values. A completely different behavior is observed at even values of M. The results for model 2 at $M = 2n$, where n is a natural number greater than 1, are found to be the same as model 5 at $M = n$. Moreover, the results for model 2 also coincide at $M = 2n$ and $M = n$ for the odd values of n.

Since the supratriangular phase has the highest configurational entropy per lattice site, it predominantly forms at even M. At the same time, only the triangular phase is observed at any integer $M/2$ in model 5. Apparently, the self-assembly mechanism of these structures realized with a gradual increase of the layer density is the same if adjusting for the scale. The coincidence of the data at odd $M/2$ is explained by the assembly of only the triangular phase in both models, but why are the remaining phases with higher entropy not being formed? The most probable supratriangular phase does not appear in model 2 at odd $M/2$ values since the unit cell size of the phase is even. The linear phase has higher entropy per site than the triangular phase only at even M, because one of the linear sizes of the unit cell has an even value. As the result, the entropy of the linear phase decreases at odd values of M in the TM simulation.

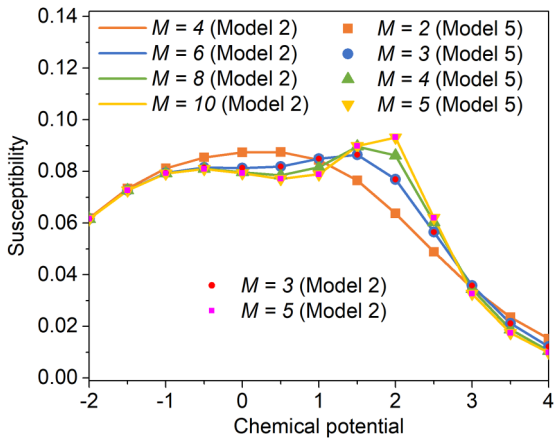

FIG. 9. Dependences of the susceptibility on the chemical potential at different M for models 2 and 5.

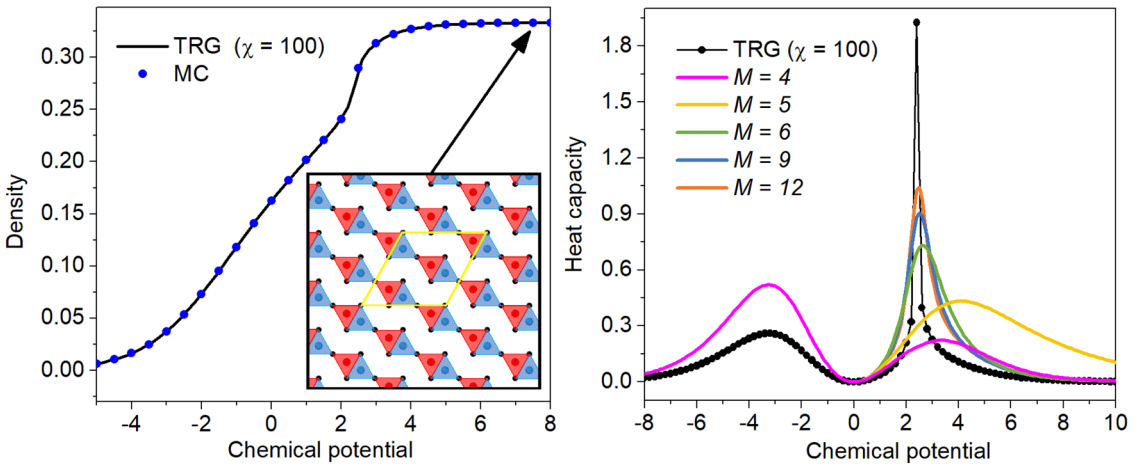

FIG. 10. Model 3: Isotherm and layer snapshot, and heat capacity of the layer vs chemical potential.

The sensitivity of the layer characteristics to odd and even values of M can be attributed to the self-assembly of triangular particles under confinement conditions: on the terraces of the high index faces of single crystals, in the narrow pores and channels, and on the surface of nanowhiskers and nanotubes.

When $M \to \infty$, the behavior of both models becomes identical. It is expressed in the same type of phase transition and position of the critical point.

Model 3. Relying on obtained data [Fig. 10], a close-packed phase in this model occurs through a continuous phase transition. It is a linear dense structure with a unit cell of 3×3 size.

Self-assembly of the ordered structure with the unit cell of 3×3 size is revealed in significantly sharper peaks of heat capacity and susceptibility calculated with the TM method at the M values that are multiples of 3. In this regard, we used only these TM ring sizes when determining the phase transition point. Using the previously found scaling relations, we have obtained the following value: $\mu_c^{\mathrm{TM}} \approx 2.41 \pm 0.01$. It is clearly seen in Fig. 10 that the TM curves tend to the curve obtained by the TRG method when M increases. The TRG method gives the following estimation of the critical chemical potential for the infinite system: $\mu_c^{\mathrm{TRG}} \approx 2.406 \pm 0.005$.

Model 4. Our calculations definitely indicate the absence of phase transitions in this model [Fig. 11].

Layer snapshots for model 4 demonstrate phase behavior similar to model 8. A close-packed phase in this model consists of a disordered mixture of differently oriented pairs of triangles contacting by an edge. Therefore, the entropy per site in this model is expectedly nonzero at $\mu \to \infty$ and gradually tends to a constant value with increasing M. Our estimation with the TM method yields the entropy value lying in the range $0.042-0.047$. This is in good agreement with the TRG calculation that gives $S^{\mathrm{TRG}} = 0.046 \pm 0.005$. These values are also very close to the entropy of the close-packed phase appearing in model 8, despite the difference in the structure of these phases. Apparently, the magnitude of the entropy of the disordered close-packed phases in models 4 and 8 is determined by the lattice geometry. Heat capacity and susceptibility of the layer as functions of the chemical potential practically coincide at $M \geqslant 8$. This confirms the absence of a phase transition in model 4.

Model 6. In this model only the c_2 configuration in which triangles have the same orientation contact by vertices is allowed. A network of co-oriented triangles is obviously formed in the model when density grows. It is confirmed

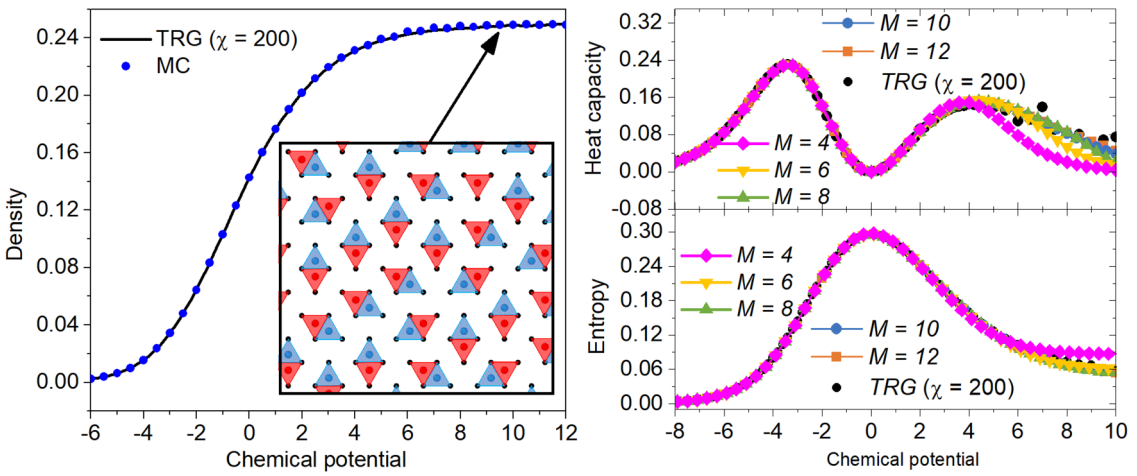

FIG. 11. Model 4: Isotherm and layer snapshot, and heat capacity and entropy of the layer vs chemical potential.

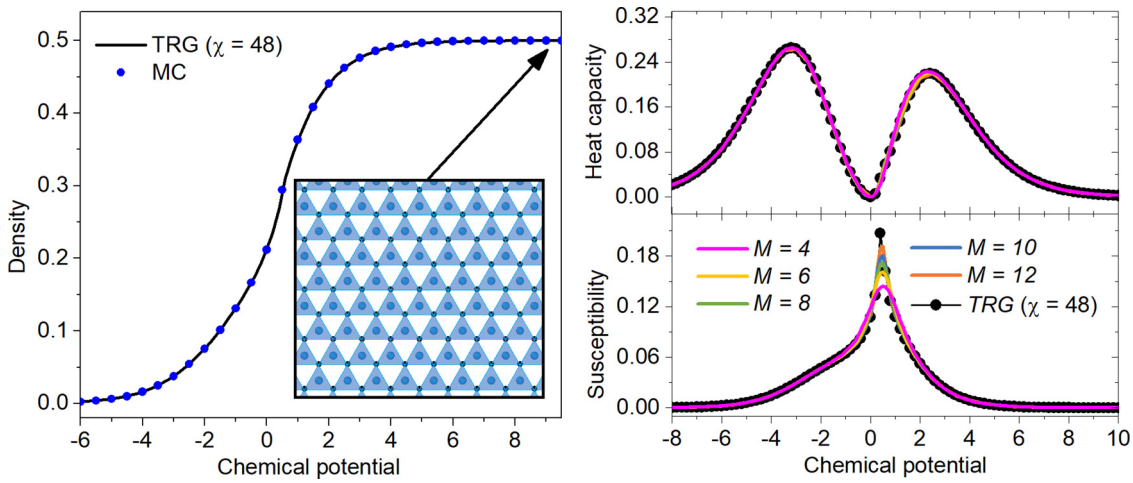

FIG. 12. Model 6: Isotherm and lattice snapshot, and graphs of heat capacity and susceptibility vs chemical potential.

by the calculated isotherm and snapshots of the layer (Fig. 12).

As one can observe, the close-packed structure in this model is the same as models 2 and 5. However, the thermodynamic characteristics of the models are different. The shape and position of the heat capacity peaks calculated with the TM method do not visibly change with increasing M, while the susceptibility peak gradually shifts. The height of the susceptibility peak gradually increases tending to the one obtained with the TRG method. The described behavior is characteristic of weak first-order phase transitions. The shift of the susceptibility maximum with increasing M is rather small. It is also a marker of a first-order phase transition. An accurate estimation of the phase transition point $\mu_c^{\mathrm{TM}} \approx 0.45 \pm 0.01$ with the TM method has been done using the scaling relations. Applying the TRG method we have gotten the following critical value: $\mu_c^{\mathrm{TRG}} \approx 0.447 \pm 0.001$.

V. CONCLUSION

Monolayers of hard particles of various shapes have been an unceasing subject of research for over 50 years. In this period two-dimensional lattice models of different hard particles from disks to Y-shaped particles and tetrominoes were extensively studied. However, the question about orientational complementarity of nonspherical particles and its effect on the structure and thermodynamic characteristics of dense phases remained open. The source of such complementarity usually arises from defectiveness or functionalization of the particle faces or molecules.

To shed light on this problem, here we have developed and investigated a series of models for reversible filling of a triangular lattice with equilateral triangles. The models differ in the set of prohibitions on specific pairs configurations. There are eight distinct models. In a zeroth approximation, these models allow one to estimate the influence of the particles' shape and complementarity of their pair configurations on the self-assembly of the dense monolayer resulting from a reversible filling.

The following main conclusions summarize the results of our study:

(i) The most symmetric models, 1, 5, 7, and 8, obtained by sequential prohibition of the pair configurations from c_1 to c_3 are equivalent to the hard-disk models on the hexagonal lattice with 1NN, 2NN, and 3NN neighbor exclusions, correspondingly. However, the structure of the close-packed layers and their phase behavior on the triangular lattice are different in all four models.

(ii) Close-packed monolayers are disordered for models 4 and 8, where any contacts of the triangles by vertices (c_2 and c_3) are prohibited. In model 8, the dense disordered phase consists of randomly oriented triangles. The close-packed phase in model 4 comprises randomly oriented pairs of triangles. There are no phase transitions in both models, and the entropy tends to the constant $S^{\mathrm{TRG}} = 0.045 \pm 0.001$ at $\mu \to \infty$. The fact is that such combination of the prohibitions eliminates a self-assembly of short- and long-range ordered structures.

(iii) In the models possessing only one prohibited pair configuration (models 2, 3, and 5) the close-packed layers are formed through the continuous phase transition. The weak first-order transition is observed in models 6 and 7, where two pair configurations are prohibited.

ACKNOWLEDGMENT

This study was supported by the Ministry of Science and Higher Education of the Russian Federation on a budget-funded basis for 2020–2022 (Project No. FSGF-2020-0001).

[1] L. Cademartiri, K. J. M. Bishop, P. W. Snyder, and G. A. Ozin, Using shape for self-assembly, Philos. Trans. R. Soc., A **370**, 2824 (2012).

[2] X. Ye, J. Chen, M. Engel, J. A. Millan, W. Li, L. Qi, G. Xing, J. E. Collins, C. R. Kagan, J. Li, S. C. Glotzer, and C. B. Murray, Competition of shape and interaction

patchiness for self-assembling nanoplates, Nat. Chem. **5**, 466 (2013).
[3] G. van Anders, D. Klotsa, N. K. Ahmed, M. Engel, and S. C. Glotzer, Understanding shape entropy through local dense packing, Proc. Natl. Acad. Sci. USA **111**, E4812 (2014).
[4] W. Xu, Z. Li, and Y. Yin, Colloidal assembly approaches to micro/nanostructures of complex morphologies, Small **14**, 1801083 (2018).
[5] D. Frenkel, Entropy-driven phase transitions, Physica A (Amsterdam, Neth.) **263**, 26 (1999).
[6] K. Zhao, R. Bruinsma, and T. G. Mason, Entropic crystal–crystal transitions of Brownian squares, Proc. Natl Acad. Sci. USA **108**, 2684 (2011).
[7] K. Zhao, R. Bruinsma, and T. G. Mason, Local chiral symmetry breaking in triatic liquid crystals, Nat. Commun. **3**, 801 (2012).
[8] S. P. Carmichael and M. S. Shell, A simple mechanism for emergent chirality in achiral hard particle assembly, J. Chem. Phys. **139**, 164705 (2013).
[9] M. Benedict and J. F. Maguire, Molecular dynamics simulation of nanomaterials using an artificial neural net, Phys. Rev. B **70**, 174112 (2004).
[10] A. P. Gantapara, W. Qi, and M. Dijkstra, A novel chiral phase of achiral hard triangles and an entropy-driven demixing of enantiomers, Soft Matter **11**, 8684 (2015).
[11] M. El Garah, A. Dianat, A. Cadeddu, R. Gutierrez, M. Cecchini, T. R. Cook, A. Ciesielski, P. J. Stang, G. Cuniberti, and P. Samorì, Atomically precise prediction of 2D self-assembly of weakly bonded nanostructures: STM insight into concentration-dependent architectures, Small **12**, 343 (2016).
[12] A. Rastgoo-Lahrood, N. Martsinovich, M. Lischka, J. Eichhorn, P. Szabelski, D. Nieckarz, T. Strunskus, K. Das, M. Schmittel, W. M. Heckl, and M. Lackinger, From Au–thiolate chains to thioether Sierpiński triangles: The versatile surface chemistry of 1,3,5-tris(4-mercaptophenyl)benzene on Au(111), ACS Nano **10**, 10901 (2016).
[13] M. E. Garah, T. R. Cook, H. Sepehrpour, A. Ciesielski, P. J. Stang, and P. Samorì, Concentration-dependent supramolecular patterns of *C*3 and *C*2 symmetric molecules at the solid/liquid interface, Colloids Surf., B **168**, 211 (2018).
[14] J. MacLeod, Design and construction of on-surface molecular nanoarchitectures: Lessons and trends from trimesic acid and other small carboxlyated building blocks, J. Phys. D: Appl. Phys. **53**, 043002 (2019).
[15] M. A. Boles, M. Engel, and D. V. Talapin, Self-assembly of colloidal nanocrystals: From intricate structures to functional materials, Chem. Rev. **116**, 11220 (2016).
[16] J. Kim, Z. Ou, M. R. Jones, X. Song, and Q. Chen, Imaging the polymerization of multivalent nanoparticles in solution, Nat. Commun. **8**, 761 (2017).
[17] H. Shen, H. Tong, P. Tan, and L. Xu, A universal state and its relaxation mechanisms of long-range interacting polygons, Nat. Commun. **10**, 1737 (2019).
[18] L. Cademartiri and G. A. Ozin, *Concepts of Nanochemistry* (John Wiley & Sons, New York, 2009).
[19] L. Cademartiri and V. Kitaev, On the nature and importance of the transition between molecules and nanocrystals: Towards a chemistry of "nanoscale perfection, Nanoscale **3**, 3435 (2011).
[20] A. Z. Panagiotopoulos, Thermodynamic properties of lattice hard-sphere models, J. Chem. Phys. **123**, 104504 (2005).
[21] H. C. M. Fernandes, J. J. Arenzon, and Y. Levin, Monte Carlo simulations of two-dimensional hard core lattice gases, J. Chem. Phys. **126**, 114508 (2007).
[22] T. Nath and R. Rajesh, Multiple phase transitions in extended hard-core lattice gas models in two dimensions, Phys. Rev. E **90**, 012120 (2014).
[23] S. S. Akimenko, V. A. Gorbunov, A. V. Myshlyavtsev, and P. V. Stishenko, Tensor renormalization group study of hard-disk models on a triangular lattice, Phys. Rev. E **100**, 022108 (2019).
[24] F. C. Thewes and H. C. M. Fernandes, Phase transitions in hard-core lattice gases on the honeycomb lattice, Phys. Rev. E **101**, 062138 (2020).
[25] T. Nath and R. Rajesh, The high density phase of the *k*-NN hard core lattice gas model, J. Stat. Mech. (2016) 073203.
[26] S. Darjani, J. Koplik, S. Banerjee, and V. Pauchard, Liquid-hexatic-solid phase transition of a hard-core lattice gas with third neighbor exclusion, J. Chem. Phys. **151**, 104702 (2019).
[27] S. Darjani, J. Koplik, V. Pauchard, and S. Banerjee, Glassy dynamics and equilibrium state on the honeycomb lattice: Role of surface diffusion and desorption on surface crowding, Phys. Rev. E **103**, 022801 (2021).
[28] W. Zhang and Y. Deng, Monte Carlo study of the triangular lattice gas with first- and second-neighbor exclusions, Phys. Rev. E **78**, 031103 (2008).
[29] A. A. A. Jaleel, J. E. Thomas, D. Mandal, Sumedha, and R. Rajesh, Rejection-free cluster Wang-Landau algorithm for hard-core lattice gases, Phys. Rev. E **104**, 045310 (2021).
[30] A. Verberkmoes and B. Nienhuis, Triangular Trimers on the Triangular Lattice: An Exact Solution, Phys. Rev. Lett. **83**, 3986 (1999).
[31] A. Verberkmoes and B. Nienhuis, Bethe ansatz solution of triangular trimers on the triangular lattice, Phys. Rev. E **63**, 066122 (2001).
[32] A. Bellemans and R. K. Nigam, Phase Transitions in the Hard-Square Lattice Gas, Phys. Rev. Lett. **16**, 1038 (1966).
[33] A. Bellemans and R. K. Nigam, Phase transitions in two-dimensional lattice gases of hard-square molecules, J. Chem. Phys. **46**, 2922 (1967).
[34] H. C. Marques Fernandes, Y. Levin, and J. J. Arenzon, Equation of state for hard-square lattice gases, Phys. Rev. E **75**, 052101 (2007).
[35] K. Ramola and D. Dhar, High-activity perturbation expansion for the hard square lattice gas, Phys. Rev. E **86**, 031135 (2012).
[36] K. Ramola, K. Damle, and D. Dhar, Columnar Order and Ashkin-Teller Criticality in Mixtures of Hard Squares and Dimers, Phys. Rev. Lett. **114**, 190601 (2015).
[37] T. Nath, D. Dhar, and R. Rajesh, Stability of columnar order in assemblies of hard rectangles or squares, Europhys. Lett. **114**, 10003 (2016).
[38] D. Mandal, T. Nath, and R. Rajesh, Estimating the critical parameters of the hard square lattice gas model, J. Stat. Mech. (2017) 043201.
[39] N. T. Rodrigues and T. J. Oliveira, Husimi-lattice solutions and the coherent-anomaly-method analysis for hard-square lattice gases, Phys. Rev. E **103**, 032153 (2021).
[40] X. Feng, H. W. J. Blöte, and B. Nienhuis, Lattice gas with nearest- and next-to-nearest-neighbor exclusion, Phys. Rev. E **83**, 061153 (2011).

[41] P. W. Kasteleyn, The statistics of dimers on a lattice: I. The number of dimer arrangements on a quadratic lattice, Physica (Amsterdam, Neth.) **27**, 1209 (1961).
[42] H. N. V. Temperley and M. E. Fisher, Dimer problem in statistical mechanics-an exact result, Philos. Mag. **6**, 1061 (1961).
[43] R. Dickman, Discontinuous phase transition in a dimer lattice gas, J. Chem. Phys. **136**, 174105 (2012).
[44] J. Kundu and R. Rajesh, Phase transitions in a system of hard rectangles on the square lattice, Phys. Rev. E **89**, 052124 (2014).
[45] J. Kundu and R. Rajesh, Asymptotic behavior of the isotropic-nematic and nematic-columnar phase boundaries for the system of hard rectangles on a square lattice, Phys. Rev. E **91**, 012105 (2015).
[46] T. Nath, J. Kundu, and R. Rajesh, High-activity expansion for the columnar phase of the hard rectangle gas, J. Stat. Phys. **160**, 1173 (2015).
[47] A. Ghosh and D. Dhar, On the orientational ordering of long rods on a lattice, Europhys. Lett. **78**, 20003 (2007).
[48] L. G. López and A. J. Ramirez-Pastor, Adsorption of self-assembled rigid rods on two-dimensional lattices, Langmuir **28**, 14917 (2012).
[49] D. A. Matoz-Fernandez, D. H. Linares, and A. J. Ramirez-Pastor, Statistical thermodynamics of long straight rigid rods on triangular lattices: Nematic order and adsorption thermodynamic functions, Langmuir **28**, 12788 (2012).
[50] J. Kundu, R. Rajesh, D. Dhar, and J. F. Stilck, Nematic-disordered phase transition in systems of long rigid rods on two-dimensional lattices, Phys. Rev. E **87**, 032103 (2013).
[51] E. E. Vogel, G. Saravia, A. J. Ramirez-Pastor, and M. Pasinetti, Alternative characterization of the nematic transition in deposition of rods on two-dimensional lattices, Phys. Rev. E **101**, 022104 (2020).
[52] D. Mandal, T. Nath, and R. Rajesh, Phase transitions in a system of hard Y-shaped particles on the triangular lattice, Phys. Rev. E **97**, 032131 (2018).
[53] R. J. Baxter, Hard hexagons: Exact solution, J. Phys. A: Math. Gen. **13**, L61 (1980).
[54] M. V. Ushcats, High-density equation of state for a lattice gas, Phys. Rev. E **91**, 052144 (2015).
[55] M. V. Ushcats, L. A. Bulavin, V. M. Sysoev, and S. J. Ushcats, Virial and high-density expansions for the Lee-Yang lattice gas, Phys. Rev. E **94**, 012143 (2016).
[56] S. Darjani, J. Koplik, and V. Pauchard, Extracting the equation of state of lattice gases from random sequential adsorption simulations by means of the Gibbs adsorption isotherm, Phys. Rev. E **96**, 052803 (2017).
[57] L. Lafuente and J. A. Cuesta, Density functional theory for nearest-neighbor exclusion lattice gases in two and three dimensions, Phys. Rev. E **68**, 066120 (2003).
[58] A. Ibenskas and E. E. Tornau, Statistical model for self-assembly of trimesic acid molecules into homologous series of flower phases, Phys. Rev. E **86**, 051118 (2012).
[59] T. Misiūnas and E. E. Tornau, ordered assemblies of triangular-shaped molecules with strongly interacting vertices: Phase diagrams for honeycomb and zigzag structures on triangular lattice, J. Phys. Chem. B **116**, 2472 (2012).
[60] V. A. Gorbunov, S. S. Akimenko, A. V. Myshlyavtsev, V. F. Fefelov, and M. D. Myshlyavtseva, Adsorption of triangular-shaped molecules with directional nearest-neighbor interactions on a triangular lattice, Adsorption **19**, 571 (2013).
[61] P. Szabelski, W. Rżysko, T. Pańczyk, E. Ghijsens, K. Tahara, Y. Tobe, and S. De Feyter, Self-assembly of molecular tripods in two dimensions: Structure and thermodynamics from computer simulations, RSC Adv. **3**, 25159 (2013).
[62] P. Szabelski, W. Rżysko, and D. Nieckarz, Directing the self-assembly of tripod molecules on solid surfaces: A Monte Carlo simulation approach, J. Phys. Chem. C **120**, 13139 (2016).
[63] W. Rżysko, D. Nieckarz, and P. Szabelski, Hierarchical ordering in adsorbed overlayers of chiral tripod molecules with directional interactions, J. Phys. Chem. C **121**, 410 (2017).
[64] P. Szabelski, D. Nieckarz, and W. Rżysko, Influence of molecular shape and interaction anisotropy on the self-assembly of tripod building blocks on solid surfaces, Colloids Surf., A **532**, 522 (2017).
[65] P. Szabelski, D. Nieckarz, and W. Rżysko, Structure formation in 2D assemblies comprising functional tripod molecules with reduced symmetry, J. Phys. Chem. C **121**, 25104 (2017).
[66] W. Rżysko, D. Nieckarz, and P. Szabelski, Modeling of the 2D self-assembly of tripod-shaped functional molecules with patchy interaction centers, Adsorption **25**, 75 (2019).
[67] E. A. Ustinov, V. A. Gorbunov, and S. S. Akimenko, Chemical potential and thermodynamic properties of self-assembled monolayers: A method of external fields in a Monte Carlo simulation, J. Phys. Chem. C **124**, 22447 (2020).
[68] C. Wang, K. Dong, and A. Yu, Structural characterization of the packings of granular regular polygons, Phys. Rev. E **92**, 062203 (2015).
[69] J.-M. Debierre and L. Turban, Critical behaviour of the hard-core lattice gas on the honeycomb lattice, Phys. Lett. A **97**, 235 (1983).
[70] L. K. Runnels, L. L. Combs, and J. P. Salvant, Exact finite method of lattice statistics. II. Honeycomb-lattice gas of hard molecules, J. Chem. Phys. **47**, 4015 (1967).
[71] S. S. Akimenko, G. D. Anisimova, A. I. Fadeeva, V. F. Fefelov, V. A. Gorbunov, T. R. Kayumova, A. V. Myshlyavtsev, M. D. Myshlyavtseva, and P. V. Stishenko, SUSMOST: Surface Science Modeling and Simulation Toolkit, J. Comput. Chem. **41**, 2084 (2020).
[72] M. Levin and C. P. Nave, Tensor Renormalization Group Approach to Two-Dimensional Classical Lattice Models, Phys. Rev. Lett. **99**, 120601 (2007).